RESEARCH ARTICLE

Construction of a three-dimensional cell culture system based on microfluidic chips

Jiaming Ma*

School of Environment and Resources, Taiyuan University of Science and Technology, Taiyuan, Shanxi, China.

Received: November 20, 2025; **accepted:** April 13, 2026.

Conventional *in vitro* cell culture often fails to recapitulate the tumor microenvironment and complex intercellular interactions. To overcome this limitation, this study developed an innovative three-dimensional (3D) cell culture system using microfluidic chip technology. The chip's microchannels were designed in Autodesk AutoCAD 2020, and polydimethylsiloxane (PDMS) chips were fabricated *via* soft lithography to enable precise droplet generation. Sodium alginate served as the matrix. By optimizing calcium chloride crosslinker concentration, uniform hydrogel microspheres were produced to provide a 3D scaffold for cells. Representative cell populations including HepG2 human hepatocellular carcinoma cells, THP-1 human acute monocytic leukemia cells, and Jurkat human T lymphocyte leukemia cells were selected *via* single-cell transcriptomic analysis and co-encapsulated within the microspheres for culture. Cell viability was assessed by using Calcein-AM/PI staining. Proliferation was measured with the Cell Counting Kit-8. Cytokine secretion was quantified by enzyme-linked immunosorbent assay. The results showed that the system reliably generated monodisperse microspheres with a diameter coefficient of variation below 3%. At 5% crosslinker concentration, microspheres fully solidified with an elastic modulus of 12.5 kPa. By day 7, the 3D microfluidic culture group exhibited an optical density of 1.68, a cell survival rate of 82.3%, and markedly increased cytokine secretion with interferon-γ and interleukin-6 levels reaching 543.2 pg/mL and 3850.4 pg/mL, respectively. Transcriptomic analysis revealed a high correlation (r = 0.75) between the 3D model and *in vivo* tissue data. This microfluidic 3D culture system effectively mimicked the tumor microenvironment and provided a robust platform for tumor immunology studies and high-throughput drug screening.

Keywords: microfluidic chip; three-dimensional cell culture; hepatocellular carcinoma; cellular microenvironment; cytokine secretion.

***Corresponding author:** Jiaming Ma, School of Environment and Resources, Taiyuan University of Science and Technology, Taiyuan, Shanxi 030024, China. Email: 18330930315@163.com.

Introduction

The tumor microenvironment is composed of diverse cell types and their secreted signaling molecules. Complex interactions among these cells play critical roles in tumor initiation, progression, and immune evasion [1]. Conventional two-dimensional (2D) cell culture systems are widely used in cell biology research. However, they fail to replicate the three-dimensional (3D) architecture and spatial interactions present *in vivo*. This limitation hinders deeper investigation into tumor biology [2]. With the rapid development of tumor immunotherapy, there is an urgent need to simulate the tumor microenvironment with high fidelity, which is particularly important for complex solid tumors such as hepatocellular carcinoma (HCC), where dynamic interactions among immune cells, tumor cells, and stromal

cells strongly influence therapeutic outcomes [3, 4]. Consequently, constructing an *in vitro* 3D cell culture system that authentically mimics the tumor microenvironment has become a major focus in both basic research and clinical translation. Microfluidic chip technology offers unique advantages for building precise 3D culture systems. Its capability for microscale fluid manipulation allows accurate control of droplet generation, cell encapsulation, and medium flow, which enables the co-culture of multiple cell types in a defined spatial environment while simultaneously monitoring cell growth dynamics and cytokine secretion in real time [5, 6]. Compared with traditional 3D culture methods such as bulk hydrogels or scaffold-based approaches, microfluidic chips improve cell proliferation efficiency and viability and maintain reproducible intercellular interactions. Moreover, these platforms can be integrated with high-throughput transcriptomic analysis to provide powerful tools for studying cellular heterogeneity, immune regulation, and tumor mechanisms, while supporting the development of personalized therapeutic strategies [7, 8].

In recent years, 3D cell culture technology has attracted widespread attention in regenerative medicine, tumor research, and drug screening. Its primary advantage is the ability to reproduce the *in vivo* microenvironment *in vitro*, providing cells with spatial structures and intercellular interactions that closely resemble physiological conditions. Killinger *et al*. used a microfluidic device to study osteoblast differentiation, demonstrating that 3D microfluidic culture promoted cell differentiation and allowed real-time monitoring of cellular function [9]. Aishwarya *et al*. reviewed dynamic 3D cell culture systems, highlighting that fluidic flow and 3D scaffolds significantly enhanced cell growth, proliferation, and metabolism, thereby improving physiological relevance and supporting high-throughput drug screening [10]. Ding *et al*. combined 3D-printed scaffold "sandwich" structures with microfluidic devices to co-culture multiple cell types, illustrating the potential of microfluidics to simulate complex *in vivo* microenvironments [11]. Zhu *et al*. incorporated micro- and nanoscale structures into 3D-printed materials, achieving precise control of drug release and enhancing carrier biocompatibility and functionality [12]. In microsphere and microchamber applications, Zhou *et al*. designed an integrated microfluidic chip for generating sodium alginate microspheres and supporting 3D cell culture. This system enabled efficient cell encapsulation and uniform distribution, thereby improving cell viability and proliferation [13]. Ko *et al*. reviewed the development of high-throughput 3D cell culture using microfluidic technology and highlighted its value for large-scale experiments and drug screening, emphasizing precise control of the cellular microenvironment and multi-parameter monitoring [14]. Dornhof *et al*. developed a microfluidic organ-on-chip platform capable of monitoring multiple analytes and tracking dynamic metabolite changes in 3D cultures. Their system provided an effective tool for *in vitro* studies of complex physiological processes [15]. The role of 3D cell culture in both basic and applied research is substantial. Biju *et al*. reported that 3D culture held unique value in drug delivery, disease modeling, and diagnostic research. By enhancing interactions between cells and the extracellular matrix, as well as intercellular interactions, 3D culture produced responses that more closely resembled *in vivo* physiology [16]. Urzì *et al*. emphasized that 3D culture bridged the gap between *in vitro* experiments and *in vivo* biological environments, overcoming the limitations of conventional 2D culture and enhancing translational relevance [17]. Li *et al*. reviewed recent advances in microfluidic chip-based 3D co-culture technology and noted that microfluidic chips allowed co-culture of multiple cell types with precise control over spatial arrangement and culture conditions. Their findings provided methodological support for tumor microenvironment simulation and studies of immune cell function [18]. Despite substantial progress in 3D cell culture and microfluidics, several challenges remain. Most studies focus on a single cell type or simple co-culture systems. Such approaches cannot fully

replicate the complex multicellular interactions in the tumor microenvironment. Existing microfluidic platforms also require improvement in encapsulation efficiency, microenvironmental uniformity, and long-term culture stability. Furthermore, few studies integrate high-throughput transcriptomic data to analyze cellular heterogeneity and validate functional outcomes. These limitations reduce the reliability of translating *in vitro* findings to *in vivo* conditions. Developing an *in vitro* model that replicates both the 3D structure and molecular characteristics of native tissue therefore remains an urgent need.

To address these current challenges, this study designed a novel 3D cell culture system based on microfluidic chip technology, targeting the hepatocellular carcinoma microenvironment by using single-cell RNA sequencing (scRNA-seq) data to guide the selection of representative cell populations and sodium alginate as the matrix material. Controlled droplet generation and precise cell encapsulation were used to produce uniform hydrogel microspheres that acted as 3D scaffolds. The microsphere structure was further optimized by adjusting the crosslinking conditions of calcium chloride ($CaCl_2$), enabling stable long-term multicellular co-culture. This biomimetic microenvironment could more accurately reflect physiological cell–cell interactions and provide a robust platform for tumor immunology research, high-throughput drug screening, and the development of personalized therapeutic strategies.

Materials and methods

Design and fabrication of the microfluidic chip

The microchannel layout was designed by using Autodesk Computer-Aided Design (AutoCAD) 2020 (https://www.autodesk.com/). The chip included three inlet channels, one flow-focusing junction, and one outlet channel. The three inlets introduced the oil phase (mineral oil as the continuous phase), the cell–sodium alginate aqueous mixture, and the $CaCl_2$ crosslinking solution. This configuration enabled continuous droplet formation and in-chip gelation. The geometric parameters of the flow-focusing region were optimized. The central aqueous channel had a width of 50 µm and delivered the cell–alginate mixture. Two side oil channels each had a width of 100 µm and provided shear to break the aqueous phase into droplets. The crosslinker inlet channel also had a width of 100 µm. After convergence, the main channel had a width of 150 µm and a uniform depth of 100 µm. This channel transported the droplets and supported their initial solidification. The design leveraged the sheath flow of oil to focus the central aqueous phase, producing highly uniform droplets. The droplet formation mechanism was characterized by the dimensionless capillary number (*Ca*) [19], which reflected the relative magnitude of viscous forces to interfacial tension and served as a key predictor of droplet formation mode and size with the calculation below.

$$Ca = \frac{\mu v}{\gamma} \quad (1)$$

where *Ca* was the capillary number. μ was the viscosity of the continuous phase. v was the characteristic velocity of the continuous phase. γ was the interfacial tension between the two phases. By precisely controlling the flow rates of both phases, the capillary number could be regulated to obtain droplets with excellent monodispersity [20]. The microfluidic chip was fabricated by using standard soft lithography techniques. A positive mold was first prepared on a silicon wafer *via* high-resolution photolithography following the design specifications described above. Polydimethylsiloxane (PDMS) monomer and crosslinker were mixed at a 10:1 mass ratio and poured over the silicon mold. The mixture was then cured in an oven at 80°C for 2 hours. After curing, the PDMS block was carefully peeled from the mold, and 1.5 mm inlet and outlet holes were created by using a puncher to serve as fluidic interfaces. The PDMS layer containing the channel structures was eventually irreversibly

Table 1. Key design parameters and functions of the microfluidic chip.

Channel Name	Width (μm)	Depth (μm)	Function
Aqueous inlet	50	100	Delivery of cell–sodium alginate mixture
Oil inlet	100	100	Delivery of continuous mineral oil phase
Crosslinker inlet	100	100	Delivery of $CaCl_2$ crosslinking solution
Flow-focusing region	50	100	Key area for droplet generation
Main channel	150	100	Droplet transport and initial solidification

bonded to an oxygen-plasma-treated glass slide, forming a closed microfluidic channel system [21]. To ensure biocompatibility and prevent nonspecific adsorption of proteins and cells, the bonded channels were passivated with a 1% Pluronic F127 solution. After soaking for one hour, the channels were dried with nitrogen and stored until use. The key design parameters and functions of the microfluidic chip were summarized in Table 1.

Establishment of the 3D cell culture system

The key aspect of constructing the 3D cell culture system was the efficient encapsulation of selected multiple cell types within sodium alginate hydrogel microspheres using the microfluidic chip to simulate cellular heterogeneity in the *in vivo* tumor microenvironment. Single-cell RNA sequencing data for hepatocellular carcinoma were obtained from the Gene Expression Omnibus (GEO) database primarily dataset GSE140228 (https://www.ncbi.nlm.nih.gov/geo/query/acc.cgi?acc=GSE140228). The data were analyzed to determine the cellular composition and gene expression features of the tumor microenvironment. Three representative cell types were selected for co-culture including HepG2 human hepatocellular carcinoma cells, THP-1 human acute monocytic leukemia cells, and Jurkat human T lymphocyte leukemia cells. All cell lines were purchased from the American Type Culture Collection (ATCC, Manassas, VA, USA). HepG2 cells were cultured in Dulbecco's Modified Eagle's medium (DMEM) (Gibco, Grand Island, NY, USA) supplemented with 10% fetal bovine serum (FBS) and 1% penicillin–streptomycin. THP-1 and Jurkat cells were maintained in Roswell Park Memorial Institute (RPMI) 1640 medium (Gibco, Grand Island, NY, USA) with the same concentrations of serum and antibiotics. All cells were incubated in a HERAcell 150i CO_2 humidified incubator (Thermo Fisher Scientific, Waltham, MA, USA) at 37°C and 5% CO_2. The aqueous and oil phases were then prepared. Sodium alginate powder (Sigma-Aldrich, St. Louis, MO, USA) was dissolved in sterile phosphate-buffered saline (PBS) to obtain a 1.5% (w/v) stock solution after sterilization by autoclaving. Cells in the logarithmic growth phase were collected and dissociated with Trypsin-EDTA. Cell numbers were determined by using a Countess II FL automated cell counter (Thermo Fisher Scientific, Waltham, MA, USA) [22]. Based on transcriptomic analysis, HepG2, THP-1, and Jurkat cells were mixed at a ratio of 7:2:1 to approximate the cellular composition of tumor tissue. The cell mixture was then resuspended in 1.0% sodium alginate solution. The final total cell concentration was adjusted to 1.0×10^7 cells/mL to ensure efficient multi-cell encapsulation within single droplets. The oil phase served as the continuous phase, which consisted of mineral oil mixed with 2% Span 80 surfactant (Sigma-Aldrich, St. Louis, MO, USA). The mixture was stirred magnetically until clear to ensure biocompatibility and droplet stability [23]. The prepared cell–sodium alginate aqueous phase, the oil phase, and $CaCl_2$ solution as a crosslinker were separately loaded into medical syringes and mounted on precision syringe pumps. Polytetrafluoroethylene tubing connected each syringe to the corresponding inlet of the microfluidic chip [24]. The size of the resulting droplets was governed through controlled modulation of the flow rate ratio between the aqueous and oil phases. Droplet formation followed the principle of volume

conservation, and the theoretical droplet diameter was estimated as follows.

$$D_{droplet} = 2 \times \sqrt{(Q_d/(\pi \times Q_c) \times W} \quad (2)$$

where $D_{droplet}$ was the droplet diameter. Q_d was the flow rate of the dispersed phase (aqueous phase). Q_c was the flow rate of the continuous phase (oil phase). W was the width of the flow-focusing channel. The generated droplets flowed into the main channel and encountered $CaCl_2$ crosslinking solution injected from the third inlet. Calcium ions diffused into the droplets and chelated with the guluronic acid residues of sodium alginate, rapidly forming a crosslinked network at the droplet interface. This process resulted in *in situ* solidification of the droplets into hydrogel microspheres within the chip [25]. The concentration of the crosslinking agent and the crosslinking duration were critical parameters that determined the structural strength and porosity of the microspheres. In this study, different $CaCl_2$ concentrations of 2.0%, 5.0%, 10.0% and crosslinking times of 2.5 min, 5.0 min, 10.0 min were evaluated to investigate their effects on gelation degree and microsphere morphology.

Cell culture and experimental design

Four experimental groups were included in this study as 3D culture system group formed by microfluidic chip-generated sodium alginate hydrogel microspheres; a conventional bulk sodium alginate hydrogel 3D culture system as the first control group, in which the cell–alginate mixture was directly dropped into $CaCl_2$ solution to form millimeter-scale hydrogels; a standard 2D culture system as the second control group, in which cells were seeded directly on conventional culture plates; and a blank microsphere group, in which cell-free hydrogel microspheres were co-cultured with cells in 2D plates to differentiate the effects of the physical 3D structure and the secretion of chemical factors. All groups were maintained in an optimized co-culture medium based on DMEM/F12 with F-12 nutrient mixture to better support multicellular growth under low-density or serum-reduced conditions. The culture medium contained 10% FBS, 1% penicillin–streptomycin, 1% non-essential amino acids, and 25 mM N-2-hydroxyethylpiperazine-N'-2-ethanesulfonic acid (HEPES) buffer to ensure stable pH throughout the culture period. On day 1, cells were stained by using a Calcein-AM/PI live/dead assay kit (Dojindo, Kumamoto, Japan) to observe initial cell viability and morphological distribution under a Leica DMi8 inverted fluorescence microscope (Leica Microsystems, Wetzlar, Germany). On day 3, culture supernatants were collected, and early cell proliferation trends were measured by using the Cell Counting Kit-8 (CCK-8, Dojindo, Kumamoto, Japan) following manufacturer's instructions. Enzyme-linked immunosorbent assay (ELISA) kits (R&D Systems, Minneapolis, MN, USA) were used to quantify the secretion levels of interleukin-6 (IL-6) and tumor necrosis factor-α (TNF-α). On Day 5, mid-stage cell proliferation and microsphere structural integrity were further assessed by using CCK-8 and microscopic observation. On Day 7, endpoint analyses were conducted including cell proliferation activity measurement, quantification of sustained cytokine secretion, and evaluation of key gene expression using quantitative polymerase chain reaction (qPCR). Cell proliferation and viability were quantitated as follows.

$$Cell\ viability\ (\%) = \frac{OD_{sample} - OD_{blank}}{OD_{control} - OD_{blank}} \times 100\% \quad (3)$$

where OD_{sample} was the absorbance of the experimental group. $OD_{control}$ was the absorbance of the control group (typically culture medium without cells). OD_{blank} was the baseline absorbance of medium without CCK-8 reagent.

Statistical analysis

All experimental data were expressed as the mean ± standard deviation (SD). Data processing and visualization were performed by using GraphPad Prism 9.0 (GraphPad Software, Boston, MA, USA). Comparisons among multiple groups were conducted by using one-way analysis of variance (ANOVA) followed by Tukey's post hoc

test for pairwise comparisons. For correlation analysis of transcriptomic data, the Pearson correlation coefficient was used to evaluate the linear correlation between the *in vitro* model and *in vivo* tissue data. *P* value less than 0.05 was considered statistically significant.

Results and discussion

Parameter regulation and size distribution of droplet generation in the microfluidic chip

Droplet generation parameters and size control of the microfluidic chip showed that the droplet diameter could be precisely tuned by adjusting the flow rates of the aqueous and oil phases. Adjusting the oil phase upward or the aqueous phase downward increased the flow rate ratio, ultimately yielding smaller droplet sizes. The coefficient of variation for droplet diameters in all experimental groups was below 3%, demonstrating excellent mono-dispersity of the generated droplets and providing a uniform and controllable microenvironment for subsequent cell encapsulation (Figure 1).

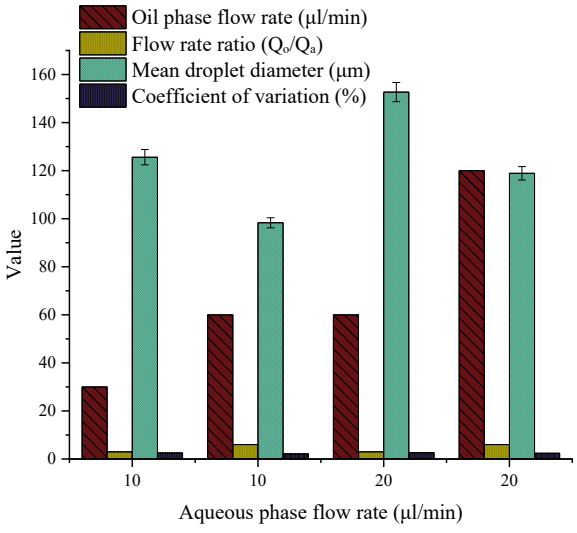

Figure 1. Droplet generation parameters and size control in the microfluidic chip.

Physical characterization of hydrogel microspheres under different crosslinking conditions

The physical properties of calcium alginate hydrogel microspheres under different crosslinking conditions demonstrated that, at a $CaCl_2$ concentration of 2.0%, gelation of the microspheres was incomplete. When the concentration increased to 10.0% or the crosslinking time extended to 10.0 min, the microspheres became excessively rigid and exhibited reduced porosity, which was unfavorable for mass transport. As the $CaCl_2$ crosslinker concentration increased from 2% to 10%, the elastic modulus of the microspheres increased significantly, while their porosity decreased correspondingly. When the crosslinker concentration was 5% and the crosslinking time was 5 minutes, the prepared microspheres displayed a spherical morphology, intact structure, and a suitable elastic modulus, achieving sufficient mechanical strength while maintaining high porosity and complete solidification (Figure 2). These conditions were identified as the optimal crosslinking parameters for subsequent cell culture experiments. The results revealed that the physical properties of calcium alginate hydrogel microspheres strongly depended on the crosslinking conditions.

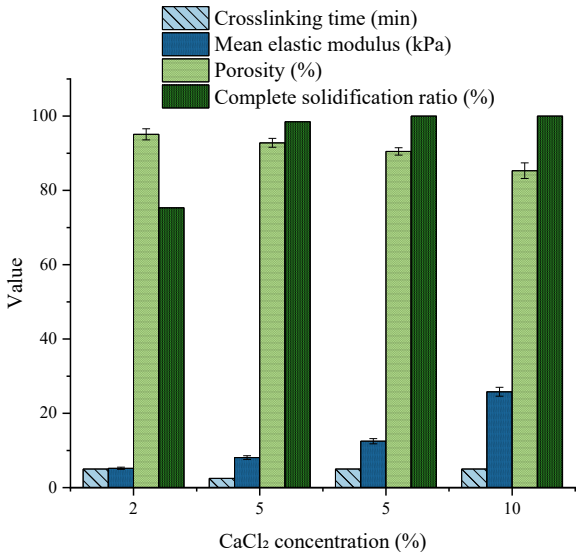

Figure 2. Physical properties of calcium alginate hydrogel microspheres under different crosslinking conditions.

Cell encapsulation efficiency and biocompatibility in the microfluidic environment

Cell encapsulation efficiency and viability in the microfluidic system demonstrated that encapsulation efficiency was positively correlated with the initial cell concentration. When the initial cell concentration increased from 2.5×10^6 to 1.0×10^7 cells/mL, the average number of cells per microsphere increased accordingly, and the encapsulation efficiency rose from 72% to 93%. Twenty-four hours after encapsulation, cell viability in all groups remained above 91%, indicating that the microfluidic encapsulation process and the microsphere environment do not adversely affect cell activity and demonstrate good biocompatibility (Figure 3).

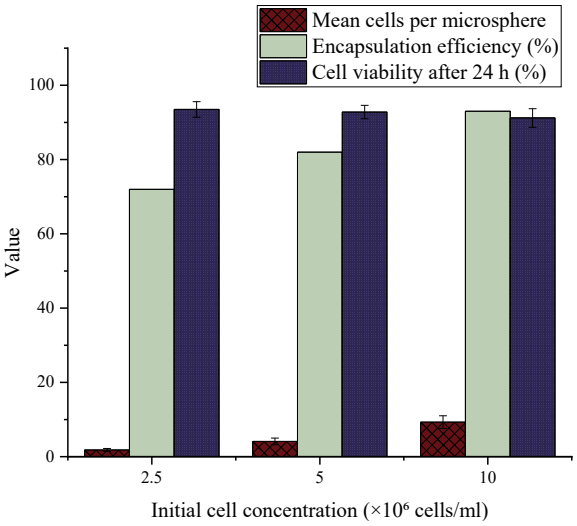

Figure 3. Statistics of microfluidic cell encapsulation efficiency and viability.

Promotion of cell proliferation and cytokine secretion by the 3D microenvironment

The comparison of cell proliferation across different culture systems showed significant differences in proliferation trends among the three culture systems. During the early culture period (days 1 – 3), absorbance values showed minimal differences across groups. As culture time extended to days 5 and 7, the CCK-8 absorbance of the 3D microfluidic microsphere group was markedly higher than that of the bulk 3D hydrogel group and the 2D co-culture group (Figure 4). This phenomenon indicated that the microfluidic-based 3D microsphere culture system most effectively promoted sustained cell proliferation.

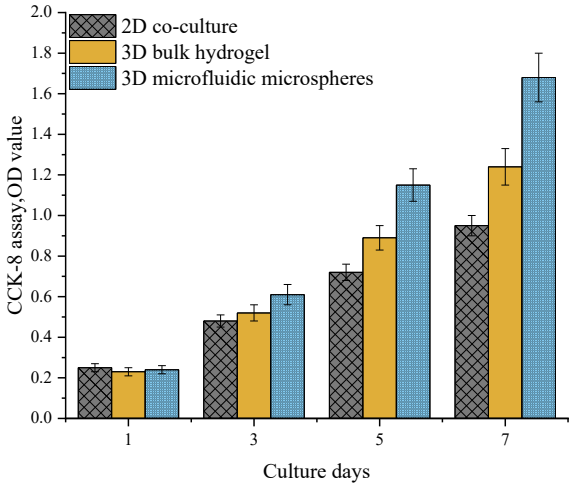

Figure 4. Comparison of cell proliferation across different culture systems.

Cytokine secretion levels in culture supernatants indicated a gradient in cytokine secretion among the three culture systems. For the three cytokines of interferon-γ (IFN-γ), TNF-α, and IL-6, the secretion levels followed the order of 3D microfluidic microsphere group > bulk 3D hydrogel group > 2D co-culture group. Among them, IL-6 exhibited the most pronounced differences between groups, suggesting that the 3D culture environment, particularly the microsphere system, enhanced cell–cell interactions and elicited stronger immune responses (Figure 5).

Transcriptomic correlation analysis between the biomimetic model and the *in vivo* microenvironment

Transcriptomic correlation analysis compared the gene expression profiles of the *in vitro* culture models with those of *in vivo* datasets. The 3D microfluidic microsphere group exhibited the highest correlation with all *in vivo* cell subpopulations including malignant cells, T cells,

and macrophages with the overall correlation coefficient reaching 0.75, markedly higher than that of the control groups (Figure 6). These results indicated that the microfluidic-based 3D co-culture model most accurately recapitulated the transcriptomic characteristics of the *in vivo* hepatocellular carcinoma microenvironment.

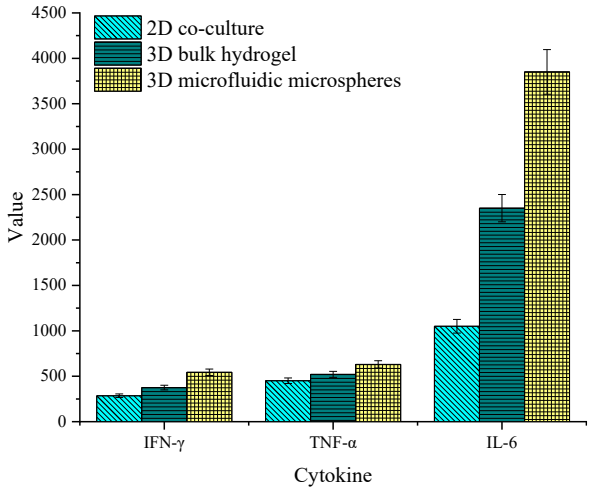

Figure 5. Cytokine secretion levels in culture supernatants.

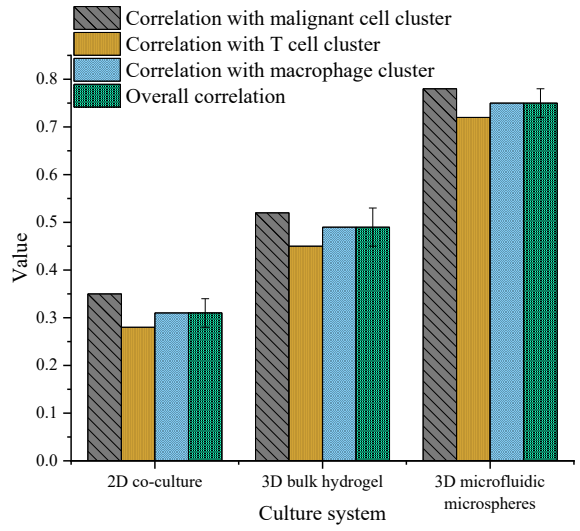

Figure 6. Transcriptomic correlation analysis.

This study successfully established a microfluidic-based 3D tumor microenvironment simulation system and demonstrated its advantages over conventional 2D and bulk 3D culture systems. The platform stably generated size-uniform calcium alginate hydrogel microspheres with tunable mechanical properties and efficiently encapsulated multiple cell types, forming a co-culture system that closely mimicked the cellular heterogeneity observed *in vivo*. Several limitations remained in this study, which included that the nutrient and metabolic waste transport in the system relied primarily on passive diffusion that could create pronounced gradients between the microsphere core and the surrounding environment, potentially affecting the viability and function of cells in deeper regions. In addition, although the model incorporated multiple cell types to partially replicate tumor heterogeneity, it lacked vascular networks, perfusion channels, and mechanical stimuli that were the components essential for a fully representative and physiologically complex microenvironment. Further, the observation period in this study was relatively short, limiting the ability to capture long-term dynamics of tumor development, cellular adaptation, and intercellular signaling. Future studies should address these limitations by incorporating vascular endothelial cells into the co-culture system to facilitate the creation of vascularized organoid models to improve nutrient and waste transport throughout the 3D structure, integrating microfluidic pump systems to simulate *in vivo* fluid shear forces and other mechanical cues to enhance physiological relevance, extending the culture duration to allow continuous monitoring of cell evolution, phenotypic changes, and intercellular interactions over longer periods. Collectively, these improvements would create a more comprehensive and physiologically accurate platform for investigation.

References

1. Badr-Eldin SM, Aldawsari HM, Kotta S, Deb PK, Venugopala KN. 2022. Three-dimensional *in vitro* cell culture models for efficient drug discovery: Progress so far and future prospects. Pharmaceuticals (Basel). 15(8):926.

2. Li X, Wang M, Davis TP, Zhang L, Qiao R. 2024. Advancing tissue culture with light-driven 3D-printed microfluidic devices. Biosensors (Basel). 14(6):301.
3. Ahn J, Ohk K, Won J, Choi DH, Jung YH, Yang JH, *et al*. 2023. Modeling of three-dimensional innervated epidermal like-layer in a microfluidic chip-based coculture system. Nat Commun. 14(1):1488.
4. Kameda Y, Chuaychob S, Tanaka M, Liu Y, Okada R, Fujimoto K, *et al*. 2022. Three-dimensional tissue model in direct contact with an on-chip vascular bed enabled by removable membranes. Lab Chip. 22(3):641-651.
5. Locatelli L, Inglebert M, Scrimieri R, Sinha PK, Zuccotti GV, Milani P, *et al*. 2022. Human endothelial cells in high glucose: New clues from culture in 3D microfluidic chips. FASEB J. 36(2):e22137.
6. Wan HY, Chen JCH, Xiao Q, Wong CW, Yang B, Cao B, *et al*. 2023. Stabilization and improved functionality of three-dimensional perfusable microvascular networks in microfluidic devices under macromolecular crowding. Biomater Res. 27(1):32.
7. Dabbagh SR, Ozdalgic B, Mustafaoglu N, Tasoglu S. 2022. Three-dimensional-bioprinted liver chips and challenges. Appl Sci (Basel). 12(10):5029.
8. Hua X, Liu X, Zhu Q, Huang P, Li Q, Liu S. 2022. Three-dimensional microfluidic chip for efficient capture of secretory autophagosomes and sensitive detection of their surface proteins. Anal Chem. 94(23):8489-8496.
9. Killinger M, Kratochvilová A, Reihs EI, Matalová E, Klepárník K, Rothbauer M. 2023. Microfluidic device for enhancement and analysis of osteoblast differentiation in three-dimensional cell cultures. J Biol Eng. 17(1):77.
10. Aishwarya P, Agrawal G, Sally J, Ravi M. 2022. Dynamic three-dimensional cell-culture systems for enhanced *in vitro* applications. Curr Sci. 122(149):149-160.
11. Ding L, Liu C, Yin S, Zhou Z, Chen J, Chen X, *et al*. 2022. Engineering a dynamic three-dimensional cell culturing microenvironment using a 'sandwich'structure-liked microfluidic device with 3D printing scaffold. Biofabrication. 14(4):045014.
12. Zhu H, Kuang H, Huang X, Li X, Zhao R, Shang G, *et al*. 2025. 3D printing of drug delivery systems enhanced with micro/nano-technology. Adv Drug Deliv Rev. 216:115479.
13. Zhou X, Zhu L, Li W. 2022. An integrated microfluidic chip for alginate microsphere generation and 3D cell culture. Anal Methods. 14(12):1181-1186.
14. Ko J, Park D, Lee J, Jung S, Baek K, E.Sung K, *et al*. 2024. Microfluidic high-throughput 3D cell culture. Nat Rev Bioeng. 2(6):453-469.
15. Dornhof J, Kieninger J, Muralidharan H, Maurer JA. Urban G, Weltin A. 2022. Microfluidic organ-on-chip system for multi-analyte monitoring of metabolites in 3D cell cultures. Lab Chip. 22(2):225-239.
16. Biju TS, Priya VV, Francis AP. 2023. Role of three-dimensional cell culture in therapeutics and diagnostics: an updated review. Drug Deliv Transl Res. 13(9):2239-2253.
17. Urzì O, Gasparro R, Costanzo E, De Luca A, Giavaresi G, Fontana S, *et al*. 2023. Three-dimensional cell cultures: The bridge between *in vitro* and *in vivo* models. Int J Mol Sci. 24(15):12046.
18. Li C, He W, Song Y, Zhang X, Sun J, Zhou Z. 2024. Advances of 3D cell co-culture technology based on microfluidic chips. Biosensors (Basel). 14(7):336.
19. Shah DD, Raghani NR, Chorawala MR, Singh SG. Prajapati B. 2023. Harnessing three-dimensional (3D) cell culture models for pulmonary infections: State of the art and future directions. Naunyn Schmiedebergs Arch Pharmacol. 396(11):2861-2880.
20. Tevlek A, Kecili S, Ozcelik OS, Kulah H, Tekin C. 2023. Spheroid engineering in microfluidic devices. ACS Omega. 8(4):3630-3649.
21. Jubelin C, Muñoz-Garcia J, Griscom L, Cochonneau D, Ollivier E, Heymann MF, *et al*. 2022. Three-dimensional *in vitro* culture models in oncology research. Cell Biosci. 12(1):155.
22. Ma Y, Hu L, Tang J, Guo W, Feng Y, Liu Y, *et al*. 2023. Three-dimensional cell co-culture liver models and their applications in pharmaceutical research. Int J Mol Sci. 24(7):6248.
23. Compera N, Atwell S, Wirth J, Törne C, Hauck SM, Meier M. 2022. Adipose microtissue-on-chip: A 3D cell culture platform for differentiation, stimulation, and proteomic analysis of human adipocytes. Lab Chip. 22(17):3172-3186.
24. Cabeza C, Rojas F, Lobos-González L, Lemaitre D, Villena J, Cordero ML, *et al*. 2025. Capture and detection of extracellular vesicles derived from human breast cancer cells using a 3D self-assembled nanostructured SiO_2 microfluidic chip. J Biol Eng. 19(1):1-17.
25. Wei WJ, Wang YC, Guan X, Chen WG, Liu J. 2022. A neurovascular unit-on-a-chip: culture and differentiation of human neural stem cells in a three-dimensional microfluidic environment. Neural Regen Res. 17(10):2260-2266.